# Delta-Kick Squeezing

Robin Corgier[1,*], Naceur Gaaloul[2], Augusto Smerzi[1], and Luca Pezzè[1]

$^{1}$*QSTAR, INO-CNR and LENS, Largo Enrico Fermi 2, 50125 Firenze, Italy*
$^{2}$*Institut für Quantenoptik, Leibniz Universität Hannover, Welfengarten 1, 30167 Hannover, Germany*

We explore the possibility to overcome the standard quantum limit (SQL) in a free-fall atom interferometer using a Bose-Einstein condensate (BEC) in either of the two relevant cases of Bragg or Raman scattering light pulses. The generation of entanglement in the BEC is dramatically enhanced by amplifying the atom-atom interactions via the rapid action of an external trap, focusing the matter waves to significantly increase the atomic densities during a preparation stage—a technique we refer to as delta-kick squeezing (DKS). The action of a second DKS operation at the end of the interferometry sequence allows one to implement a nonlinear readout scheme, making the sub-SQL sensitivity highly robust against imperfect atom counting detection. We predict more than 30 dB of sensitivity gain beyond the SQL for the variance, assuming realistic parameters and $10^6$ atoms.

Free-fall atom interferometers [1–3] are extraordinarily sensitive to external forces and find key applications as gravimeters, gradiometers, and gyroscopes in applied physics and fundamental science [4–6]. State-of-the-art devices use $N$ uncorrelated atoms and their phase estimation uncertainty is lower bounded by the standard quantum limit (SQL), $\Delta\theta_{\text{SQL}} = 1/\sqrt{N}$. Since $N$ is generally constrained by the experimental apparatus or by the onset of unwanted systematic effects due to the high density, the possibility to overcome the SQL by engineering specific quantum correlations [7] between the atoms is attracting increasing interest [8].

Entanglement-enhanced atom interferometry [8–13] has mainly focused on atomic clocks [14–20] and magnetometers [21–26]. Free-fall atom interferometers have received less attention [27–33]. The main reason is that these measurement devices have stringent practical requirements: in particular, the generation of atomic entanglement must be compatible with the splitting of the atomic wave packets in momentum modes. Bose-Einstein condensates (BECs) have been pinpointed as optimal candidates for the realization of entanglement-enhanced free-fall atom interferometers 31]]. Indeed, the narrow momentum dispersion guarantees ideal splitting [34] and entanglement can be generated via particle-particle interactions [8–10,31–33,35,36]. However, since the interaction vanishes due to free-fall expansion, current theoretical studies predict only a modest sub-SQL sensitivity gain [31].

In this Letter, we overcome these limitations by proposing a novel method to enhance the generation of entanglement in free-fall atom interferometers using BECs. The key idea consists of focusing the matter waves through the rapid application of an external trapping potential in analogy to optics, where the trap plays the role of a converging lens.

Going through the focal point increases the matter-wave density and thus the effective strength of the particle-particle interactions preparing the atoms in a highly entangled spin-squeezed state. Considering previous works on delta-kick collimation [37–42], we designate our technique "delta-kick squeezing" (DKS). The method is explored for Raman and Bragg scattering and is made fully compatible with the requirement of linear atom interferometer operations. The DKS technique leads to a substantial phase sensitivity gain beyond the SQL, e.g., more than 30 dB in a realistic experimental configuration with $10^6$ atoms. For Bragg diffraction, in particular, using a second DKS pulse at the end of the interferometer sequence allows the realization of a nonlinear readout protocol [43–51]. In this case, the twisting dynamics generating the spin-squeezed state is inverted before the final measurement of the atom number in the two interferometer output ports. This operation makes the interferometer exceptionally robust against detection noise.

*DKS state preparation protocol.*—The preparation step illustrated in Fig. 1(a) starts with a BEC suddenly released from an external trap. A short free expansion time $T_0$ dilutes the BEC and guarantees, by applying a first beam splitter pulse (BS1), the preparation of the quantum superposition $|\psi_0\rangle = (|g\rangle + |e\rangle)^{\otimes N}/2^{N/2}$, with $N$ being the number of atoms and $|g\rangle$ and $|e\rangle$ two momentum states [52]. Entanglement is then generated via particle-particle interactions in the BEC, such that $|\psi_0\rangle$ evolves according to the one-axis twisting dynamics $|\psi_{\text{sq}}(t)\rangle = e^{-i\tau(t)\hat{S}_z^2}|\psi_0\rangle$ [35,36,53], where $\tau(t) = \int_0^t \chi(t')dt'$. Notably, the time-dependent nonlinear coefficient $\chi(t)$ is given by [54]

$$\chi^R(t) = \chi_S(t) - \chi_C(t), \tag{1a}$$
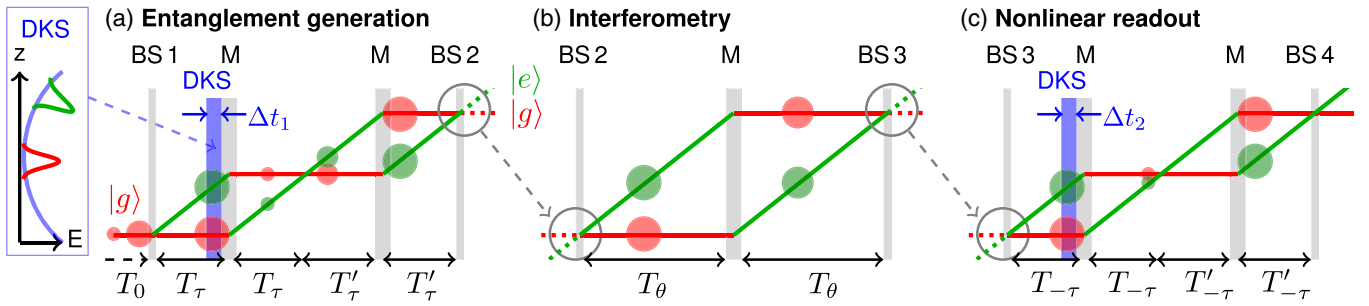
FIG. 1. Complete operation of a DKS-enhanced free-fall atom interferometer. State preparation (a) consists of (i) a first expansion of the BEC $T_0$, (ii) a beam splitter (BS1), (iii) a DKS of duration $\Delta t_1$ focusing the matter waves (inset), and (iv) two mirror pulses (M). The interferometer sequence (b) starts with the beam splitter (BS2) followed by a mirror (M) and ending with a recombining beam splitter (BS3). The pulses are equally separated in time by $T_\theta$. In a linear detection scheme, the phase is evaluated by counting the number of atoms at the two output ports. In a nonlinear readout case (c), one applies operations analog to the state preparation. Right before the first mirror pulse, a second DKS of duration $\Delta t_2$ is applied and generates an "untwisting" dynamics. The phase is finally evaluated by counting the number of atoms at the two output ports.

$$\chi^B(t) = \chi_S(t) - 2\chi_C(t), \tag{1b}$$

for the Raman ($R$) or the Bragg ($B$) scattering, respectively. Here, $\chi_S(t) = g \int_{-\infty}^{\infty} d\mathbf{r}|\phi_{g(e)}(\mathbf{r},t)|^4/\hbar$ and $\chi_C(t) = g \int_{-\infty}^{\infty} d\mathbf{r}|\phi_g(\mathbf{r},t)|^2|\phi_e(\mathbf{r},t)|^2/\hbar$ denote the self-phase- and cross-phase-modulation terms, respectively, where, $\phi_{g(e)}(\mathbf{r},t)$ carries the spatial evolution of the state $|g\rangle$ ($|e\rangle$) and are calculated here within a Thomas-Fermi approximation [54]. For simplicity, in the following we assume the same intra- and inter-species scattering coefficient $g = g_{11} = g_{12} = g_{22} > 0$ [58]. The factor 2 in front of the cross-phase-modulation terms in Eq. (1b) [59,60] is due to the interference of the two modes [54] and is of rich consequence. In particular, when the wave functions overlap, $\chi_S$ and $\chi_C$ are equal and thus $\chi^R \approx 0$ in the Raman case [9,10]. In contrast, during overlap, $\chi^B \approx -\chi_S \neq 0$, making the one-axis twisting evolution active in the Bragg case. Furthermore, $\chi^B$ can assume either positive or negative values (see below), while $\chi^R \geq 0$.

The atomic interactions, proportional to the density of the freely expanding cloud, are vanishing a few milliseconds after release and therefore prohibit the generation of highly entangled states [31]. This problem is overcome here by switching on, after a preexpansion time $t_{\mathrm{exp}}$, a harmonic trap for a time $\Delta t$. This external potential, created with a single dipole trap [61,62], encompasses the two spatial modes. It induces a size refocusing that increases the density of the atomic clouds [Fig. 2(a)] [63] and thus the effective interaction coefficient $\tau$. Right after the delta-kick pulse, at time $T_\tau = t_{\mathrm{exp}} + \Delta t_1$, a first mirror pulse (M) is applied. The DKS pulse leads to an extra relative phase between the two modes [64–66]. A detailed discussion of its impact and compensation techniques can be found in [54]. The state preparation stage ends after an additional time $2T'_\tau$, where $T'_\tau$ can be tuned depending on the specific DKS parameters to

guarantee noninteracting clouds and linear interferometers sequences. Figures 2(a)–2(c) present a realistic example of state preparation using the DKS [67]: we show the size of the BEC cloud in Fig. 2(a) and the nonlinear coefficient $\chi$ as a function of time in Fig. 2(b). The latter clearly shows how $\chi(t)$ is enhanced by the DKS and is different for Raman and Bragg pulses. Figure 2(c) shows $\tau$ as a function of the DKS pulse duration $\Delta t$. In particular, for Bragg scattering, $\tau$ can have either positive or negative values, depending on $\Delta t$.

*Atom interferometry with linear readout.*—The Mach-Zehnder interferometer sequence illustrated in Fig. 1(b) consists of two beam splitters (BS2 and BS3) and a mirror pulse (M) equally spaced in time by $T_\theta$. We define the sensitivity gain over the standard quantum limit $\mathcal{G} = \Delta\theta_{\mathrm{SNL}}/\Delta\theta$ calculated at $\theta = 0$ [68], where $\theta$ denotes the phase accumulated during the interferometer and $(\Delta\theta)^2 = (\Delta S_z)^2/(d\langle S_z\rangle/d\theta|_{\theta=0})^2$ is obtained by error propagation [69]. In the case of an ideal linear interferometer, i.e., $\tau_{\mathrm{AI}} = \int_{T_i}^{T_i+2T_\theta} \chi(t')dt' = 0$, with $T_i = T_0 + 2T_\tau + 2T'_\tau$, the output state reads $|\psi_{\mathrm{out}}\rangle = \hat{U}_{\mathrm{AI}}|\psi_{\mathrm{sq}}\rangle$ with $\hat{U}_{\mathrm{AI}} = e^{i\theta\hat{S}_y}$ [69]. The sensitivity gain reads

$$\mathcal{G} = \frac{2\cos(\tau)^{N-1}}{[4 + (N-1)(A - \sqrt{A^2 + B^2})]^{1/2}}, \tag{2}$$

with $A = 1 - \cos(2\tau)^{N-2}$ and $B = 4\sin(\tau)\cos(\tau)^{N-2}$, upon an opportune rotation [36] of the squeezed state $|\psi_{\mathrm{sq}}(t)\rangle$ at BS2. The maximum value of $\mathcal{G}$ is reached for $\tau_{\mathrm{opt}} \approx 1.2N^{-2/3}$ [7,36]. In Figs. 2(d) and 2(e), we plot the gain $\mathcal{G}$ as a function of the DKS parameters $t_{\mathrm{exp}}$ and $\Delta t$, for Bragg and Raman scattering, respectively. While for $\Delta t = 0$, no significant gain can be obtained ($\mathcal{G} \approx 1$), the DKS enables the creation of highly entangled input states in these freely expanding configurations: a large gain is possible depending on $t_{\mathrm{exp}}$ and $\Delta t$.
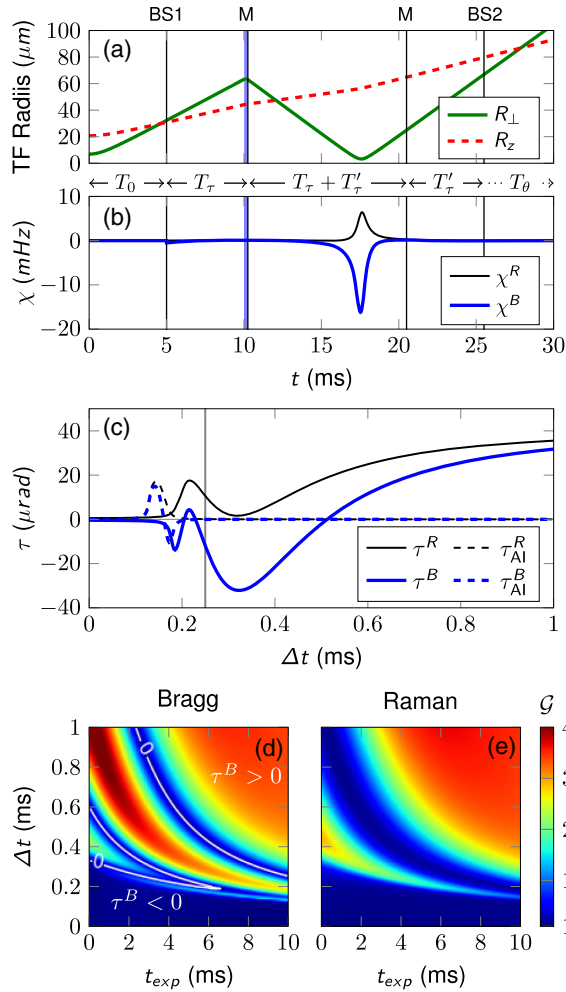
FIG. 2. DKS engineering. (a) Thomas-Fermi (TF) Radii along the $z$ ($R_z$) and transverse directions ($R_\perp$) as a function of time during state preparation [67]. The different laser pulses are highlighted by the vertical black lines with $T_\tau = T'_\tau = 5.25$ ms and the DKS time is fixed to $\Delta t = 0.25$ ms (vertical blue lines). (b) Corresponding nonlinear coefficient $\chi(t)$ for Raman and Bragg scattering. (c) Effective nonlinear coefficient $\tau$ as a function of the DKS duration $\Delta t$, during the state preparation (solid lines) and during the interferometer sequence (dashed). The vertical line denotes the case shown in (a) and (b). (d),(e) The sensitivity gain $\mathcal{G}$ (color scale) for the Bragg (d) and Raman (e) configurations as a function of the preexpansion time and DKS duration. The white lines denote $\tau^B = 0$ and we distinguish regions with $\tau^B > 0$ and $\tau^B < 0$. Here, $\mathcal{G} = 40$ corresponds to a variance of 32 dB below the SQL.

*Atom interferometry with nonlinear readout.*—Using the DKS to tune the sign of the effective interaction for Bragg scattering can be exploited to realize a nonlinear readout scheme. After the interferometer sequence, a second DKS is applied, see Fig. 1(c), such that the output state is now given by

$$|\psi_{\rm out}\rangle = e^{-i\pi/2\hat{S}_y} e^{-i\tau_2\hat{S}_z^2} \hat{U}_{\rm AI} e^{-i\tau_1\hat{S}_z^2} |\psi_0\rangle. \tag{3}$$

Notice that the final rotation $e^{-i\pi/2\hat{S}_y}$ is not included in Fig. 1. We now distinguish the sensitivity gain of the linear detection $\mathcal{G}$ to the nonlinear readout $\mathcal{Q}$. In the case where

$$\tau_1 = -\tau_2 \equiv \tau \tag{4}$$

and $\theta = 0$, the nonlinear readout provides (i) the possibility to reach a higher sensitivity gain, $\max(\mathcal{Q}) > \max(\mathcal{G})$, with respect to the linear detection case for sufficiently large values of $\tau$ [Fig. 3(a)] [44], and (ii) a phase magnification robust against the imperfect detection of the atom number [Fig. 3(b)] [44,47]. The latter being one of the most critical limitations in quantum-enhanced atom interferometers [8]. Throughout this Letter, the imperfect detection resolution is modeled by a Gaussian noise of variance $(\Delta n)^2$ [8,31].

Satisfying the condition (4) is not straightforward in quantum systems, as it requires inverting the twisting evolution that generated entanglement in the probe state. Such a possibility has been predicted for Rydberg atoms [44,46] and realized for cold atoms in a cavity [47] and trapped ions [43,71]. Here the condition (4) can be naturally satisfied by using Bragg scattering and tuning
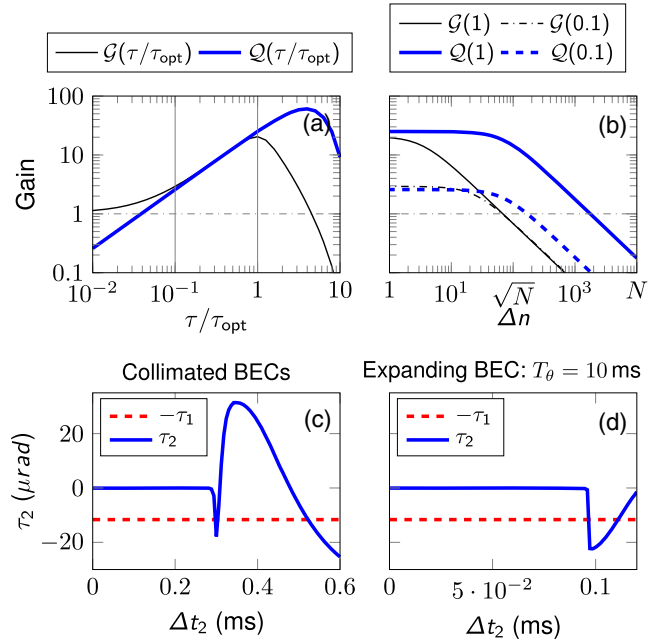


FIG. 3. Nonlinear readout. (a) Sensitivity gain for linear $\mathcal{G}(\tau/\tau_{\rm opt})$ and nonlinear $\mathcal{Q}(\tau/\tau_{\rm opt})$ readout as a function of the effective nonlinear coefficient, $\tau = \tau_1 = -\tau_2$. The vertical lines denote $0.1\tau_{\rm opt}$ and $\tau_{\rm opt}$. (b) Sensitivity gain as a function of the detection noise $\Delta n$ for linear and nonlinear readout, $\tau = \tau_{\rm opt}$ (solid) and $\tau = 0.1\tau_{\rm opt}$ (dashed). The number of atoms is $N = 10^4$. (c),(d) The nonlinear coefficient as a function of the second DKS duration $\Delta t_2$ (solid blue line). The size of the BECs are assumed to be constant after BS2 in (c) while they continue to expand after BS2 in (d). For specific values of $\Delta t_2$, the nonlinear coefficient matches $-\tau_1 \approx -0.1\tau_{\rm opt}$ [70].

the DKS parameters. This is shown in Figs. 3(c) and 3(d) where we plot $\tau_2$ as a function of the DKS durations $\Delta t_2$ and compare it to $-\tau_1$ for different $T_\theta$. The condition (4) can be satisfied in realistic experimental conditions. In particular, Fig. 3(c) shows the case where the sizes of the BECs are kept constant after BS2 until the second DKS during the nonlinear readout. This configuration can be engineered through the action of a delta-kick collimation pulse [37–42] before BS2 when the two clouds are dilute enough. This manipulation leads to record low-expansion rates as low as 50 pK [40,42], enabling interferometer sequences longer than $T_\theta = 1$ s. In this configuration, $\Delta t_2$ is independent of $T_\theta$ and allows one to perfectly "untwist" the state with a second DKS pulse of some hundreds of microseconds. In the case where the BECs kept expanding after BS2, Fig. 3(c) can be interpreted as $T_\theta = 0$ and increased $T_\theta$ requires shorter DKS pulse [Fig. 3(d)]. In Fig. 4(a), we give a more complete overview of the nonlinear readout parameters beyond the condition (4). There, we plot the sensitivity gain $\mathcal{Q}$ as a function of $\tau_1$ and $-\tau_2$. Slight unbalanced conditions (namely, $|\tau_1 + \tau_2| \gtrsim 0$) still enable high sensitivity gains.

*Impact of residual mean-field interactions.*—In the presence of a small residual interaction after the state preparation, the interferometer transformation is described



FIG. 4. Robustness of the nonlinear readout. Interferometer sensitivity gain as a function of $\tau_1$ and $\tau_2$ for linear ($\mathcal{Q}^L$) (a) and nonlinear ($\mathcal{Q}^{NL}$) interferometer sequence with $\tau_{AI} = 10\%\tau_1$ (b) and $\tau_{AI} = -10\%\tau_1$ (c). Here $\mathcal{Q} = 10(3)$ correspond to a variance of 20 (9.5) dB below the SQL. (d) Sensitivity gain as a function of $\tau = \tau_1 = -\tau_2$. The case $\tau = 0.1\tau_{opt}$ corresponds to the circles in (a)–(c) and is highlighted by the vertical line. (e) Sensitivity gain as a function of the detection noise parameter $\Delta n$ and for $\tau = 0.1\tau_{opt}$. In all $N = 10^3$.

by $\hat{U}_{AI} = e^{i\theta\hat{S}_y} e^{i\tau_{AI}\hat{S}_y^2}$ in Eq. (3). While the interactions during the interferometer largely degrade the sensitivity gain in a linear detection scheme ($\mathcal{G}^{NL} \leq \mathcal{G}^L$ [60], the labels L and NL distinguish between a linear and nonlinear interferometer sequence, respectively), this is surprisingly not the case when exploiting the nonlinear readout. In Figs. 4(b) and 4(c), we plot $\mathcal{Q}^{NL}$ as a function of $\tau_1$ and $-\tau_2$ for $\tau_{AI} = \pm 0.1\tau_1$ and contrast it to the linear case ($\mathcal{Q}^L$, for $\tau_{AI} = 0$) in Fig. 4(a). We conclude that sub-shot-noise sensitivities are obtained for a small imbalance between $\tau_1$ and $-\tau_2$ when $\text{sign}(\tau) \neq \text{sign}(\tau_{AI})$ [Fig. 4(b)] or large imbalance when $\text{sign}(\tau) = \text{sign}(\tau_{AI})$ [Fig. 4(c)]. To emphasize these results, we plot in Fig. 4(d) the sensitivity gain for the specific case, $\tau_1 = -\tau_2$. Here if $\text{sign}(\tau) \neq \text{sign}(\tau_{AI})$, we find a parameter range where $\mathcal{Q}^{NL} \geq \mathcal{Q}^L > 1$, while if $\text{sign}(\tau) = \text{sign}(\tau_{AI})$, $\mathcal{Q}^{NL} < \mathcal{Q}^L$. This result is confirmed analytically in the regime of low interactions where [54]

$$(\mathcal{Q}^{NL})^2 = \frac{1}{4}\left[(4\tau - 3\tau_{AI})\frac{N}{2} - (2\tau - \tau_{AI})\right]^2. \quad (5)$$

In Fig. 4(e), we plot the corresponding robustness to atom number resolution of the nonlinear readout for $\tau = 0.1\tau_{opt}$ and verify that there is no significant gain difference between the different configurations. While the presence of residual interactions and imperfect detection prohibit sub-SQL sensitivity with linear detection schemes, nonlinear readout enables the creation of a quantum-enhanced interferometer sequence, in the regime of low interactions, robust against imperfect detection.

*Conclusions and discussion.*—In this Letter, we have proposed and studied a phase-space engineering technique to focus matter waves that (i) substantially enhances the amount of entanglement in a free-fall atom interferometer and (ii) realizes, with Bragg diffraction, a nonlinear readout protocol making the interferometer sensitivity extraordinarily robust against detection noise. This robustness is crucial in atom interferometers with nonclassical states to avoid dramatic effects of imperfect atom number detection on sub-SQL sensitivities. While it is also possible to tune the atomic scattering length across a Feshbach resonance with external magnetic field, the DKS technique has the key advantage of being independent from the scattering length, sensitivity to magnetic field, and initial density of the atomic clouds. Furthermore, the realization of nonlinear readout scheme with Feshbach field would require one to tune the $s$-wave scattering length from repulsive to attractive interactions and may induce BEC collapse.

Our predictions have been obtained for realistic experimental parameters and assuming ideal beam splitter and mirror pulses. Different effects may degrade the sensitivity of the interferometer as atomic losses [72,73], mode mismatch [74], and shape deformation [75], due to BEC crossing and residual interaction during splitting pulses [76]. A careful analysis of these effects depends

on the specific interferometer configuration and is beyond the scope of this work. The assumption of harmonic traps to realize the DKS is justified for BEC sizes and the proposed spatial separations. Within these assumptions, a sensitivity gain of more than 30 dB beyond the SQL with $10^6$ atoms is predicted for both Bragg and Raman diffraction. Larger harmonic traps [61,62] could enable even higher sensitivity gains.

Our technique can boost the sensitivity of a BEC gravimeter [77,78] of $10^6$ atoms to that of an ensemble with a 100-fold flux. Our DKS technique thus promotes BEC ensembles in free-fall atom interferometers to primary quantum-enhanced sensors to explore timely physics quests such as testing general relativity principles [79,80] or atom-interferometric gravitational-wave detection [81].

* robin.corgier@gmail.com

[1] P. R. Berman, *Atom Interferometry* (Academic Press, San Diego, 1997).

[2] A. D. Cronin, J. Schmiedmayer, and D. E. Pritchard, Optics and interferometry with atoms and molecules, Rev. Mod. Phys. **81**, 1051 (2009).

[3] G. M. Tino and M. A. Kasevich, Atom Interferometry in *Proceedings of the International School of Physics "Enrico Fermi," Course CLXXXVIII* (Societá Italiana di Fisica, Bologna, 2014).

[4] M. S. Safronova, D. Budker, D. DeMille, D. F. J. Kimball, A. Derevianko, and C. W. Clark, Search for new physics with atoms and molecules, Rev. Mod. Phys. **90**, 025008 (2018).

[5] K. Bongs, M. Holynski, J. Vovrosh, P. Bouyer, G. Condon, E. Rasel, C. Schubert, W. P. Schleich, and A. Roura, Taking atom interferometric quantum sensors from the laboratory to real-world applications, Nat. Rev. Phys. **1**, 731 (2019).

[6] R. Geiger, A. Landragin, S. Merlet, and F. Pereira Dos Santos, High-accuracy inertial measurements with cold-atom sensors, AVS Quantum Sci. **2**, 024702 (2020).

[7] L. Pezzè and A. Smerzi, Entanglement, Nonlinear Dynamics, and the Heisenberg Limit, Phys. Rev. Lett. **102**, 100401 (2009).

[8] L. Pezzè, A. Smerzi, M. K. Oberthaler, R. Schmied, and P. Treutlein, Quantum metrology with nonclassical states of atomic ensembles, Rev. Mod. Phys. **90**, 035005 (2018).

[9] C. Gross, T. Zibold, E. Nicklas, J. Estève, and M. K. Oberthaler, Nonlinear atom interferometer surpasses classical precision limit, Nature (London) **464**, 1165 (2010).

[10] M. F. Riedel, P. Böhi, Y. Li, T. W. Hänsch, A. Sinatra, and P. Treutlein, Atom-chip-based generation of entanglement for quantum metrology, Nature (London) **464**, 1170 (2010).

[11] B. Lücke *et al.*, Twin matter waves for interferometry beyond the classical limit, Science **334**, 773 (2011).

[12] O. Hosten, N. J. Engelsen, R. Krishnakumar, and M. A. Kasevich, Measurement noise 100 times lower than the quantum-projection limit using entangled atoms, Nature (London) **529**, 505 (2016).

[13] J. G. Bohnet, K. C. Cox, M. A. Norcia, J. M. Weiner, Z. Chen, and J. K. Thompson, Reduced spin measurement back-action for a phase sensitivity ten times beyond the standard quantum limit, Nat. Photonics **8**, 731 (2014).

[14] A. Louchet-Chauvet, J. Appel, J. J. Renema, D. Oblak, N. Kjaergaard, and E. S. Polzik, Entanglement-assisted atomic clock beyond the projection noise limit, New J. Phys. **12**, 065032 (2010).

[15] I. D. Leroux, M. H. Schleier-Smith, and V. Vuleti, Orientation-Dependent Entanglement Lifetime in a Squeezed Atomic Clock, Phys. Rev. Lett. **104**, 250801 (2010).

[16] I. Kruse, K. Lange, J. Peise, B. Lücke, L. Pezzè, J. Arlt, W. Ertmer, C. Lisdat, L. Santos, A. Smerzi, and C. Klempt, Improvement of an Atomic Clock Using Squeezed Vacuum, Phys. Rev. Lett. **117**, 143004 (2016).

[17] E. Pedrozo-Peñafiel, S. Colombo, C. Shu, A. F. Adiyatullin, Z. Li, E. Mendez, B. Braverman, A. Kawasaki, D. Akamatsu, Y. Xiao, and V. Vuletić, Entanglement on an optical atomic-clock transition, Nature (London) **588**, 414 (2020).

[18] A. André, A. S. Sørensen, and M. D. Lukin, Stability of Atomic Clocks Based on Entangled Atoms, Phys. Rev. Lett. **92**, 230801 (2004).

[19] M. Schulte, C. Lisdat, P. O. Schmidt, U. Sterr, and K. Hammerer, Prospects and challenges for squeezing-enhanced optical atomic clocks, Nat. Commun. **11**, 5955 (2020).

[20] L. Pezzè and A. Smerzi, Heisenberg-Limited Noisy Atomic Clock Using a Hybrid Coherent and Squeezed State Protocol, Phys. Rev. Lett. **125**, 210503 (2020).

[21] V. Petersen, L. B. Madsen, and K. Mølmer, Magnetometry with entangled atomic samples, Phys. Rev. A **71**, 012312 (2005).

[22] W. Wasilewski, K. Jensen, H. Krauter, J. J. Renema, M. V. Balabas, and E. S. Polzik, Quantum Noise Limited and Entanglement-Assisted Magnetometry, Phys. Rev. Lett. **104**, 133601 (2010).

[23] R. J. Sewell, M. Koschorreck, M. Napolitano, B. Dubost, N. Behbood, and M. W. Mitchell, Magnetic Sensitivity beyond the Projection Noise Limit by Spin Squeezing, Phys. Rev. Lett. **109**, 253605 (2012).

[24] C. F. Ockeloen, R. Schmied, M. F. Riedel, and P. Treutlein, Quantum Metrology with a Scanning Probe Atom Interferometer, Phys. Rev. Lett. **111**, 143001 (2013).

[25] W. Muessel, H. Strobel, D. Linnemann, D. B. Hume, and M. K. Oberthaler, Scalable Spin Squeezing for

Quantum-Enhanced Magnetometry with Bose-Einstein Condensates, Phys. Rev. Lett. 113, 103004 (2014).

[26] T. Ruster, H. Kaufmann, M. A. Luda, V. Kaushal, C. T. Schmiegelow, F. Schmidt-Kaler, and U. G. Poschinger, Entanglement-Based dc Magnetometry with Separated Ions, Phys. Rev. X 7, 031050 (2017).

[27] S. A. Haine, Information-Recycling Beam Splitters for Quantum Enhanced Atom Interferometry, Phys. Rev. Lett. 110, 053002 (2013).

[28] P. Hamilton, M. Jaffe, J. M. Brown, L. Maisenbacher, B. Estey, and H. Müller, Atom Interferometry in an Optical Cavity, Phys. Rev. Lett. 114, 100405 (2015).

[29] L. Salvi, N. Poli, V. Vuletić, and G. M. Tino, Squeezing on Momentum States for Atom Interferometry, Phys. Rev. Lett. 120, 033601 (2018).

[30] A. Shankar, L. Salvi, M. L. Chiofalo, N. Poli, and M. J. Holland, Squeezed state metrology with Bragg interferometers operating in a cavity, Quantum Sci. Technol. 4, 045010 (2019).

[31] S. S. Szigeti, S. P. Nolan, J. D. Close, and S. A. Haine, High-Precision Quantum-Enhanced Gravimetry with a Bose-Einstein Condensate, Phys. Rev. Lett. 125, 100402 (2020).

[32] F. Anders et al., Momentum Entanglement for Atom Interferometry, Phys. Rev. Lett. 127, 140402 (2021).

[33] S. S. Szigeti, O. Hosten, and S. A. Haine, Improving cold-atom sensors with quantum entanglement: Prospects and challenges, Appl. Phys. Lett. 118, 140501 (2021).

[34] S. S. Szigeti, J. D. Debs, J. J. Hope, N. P. Robins, and J. D. Close, Why momentum width matters for atom interferometry with Bragg pulses, New J. Phys. 14, 023009 (2012).

[35] A. Sørensen, L.-M. Duan, J. I. Cirac, and P. Zoller, Many-particle entanglement with Bose-Einstein condensates, Nature (London) 409, 63 (2001).

[36] M. Kitagawa and M. Ueda, Squeezed spin states, Phys. Rev. A 47, 5138 (1993).

[37] S. Chu, J. E. Bjorkholm, A. Ashkin, J. P. Gordon, and L. W. Hollberg, Proposal for optically cooling atoms to temperatures of the order of $10^{-6}$ K, Opt. Lett. 11, 73 (1986).

[38] H. Ammann and N. Christensen, Delta Kick Cooling: A New Method for Cooling Atoms, Phys. Rev. Lett. 78, 2088 (1997).

[39] H. Müntinga, H. Ahlers, M. Krutzik, A. Wenzlawski, S. Arnold, B. Becker et al., Interferometry with Bose-Einstein Condensates in Microgravity, Phys. Rev. Lett. 110, 093602 (2013).

[40] T. Kovachy, J. M. Hogan, A. Sugarbaker, S. M. Dickerson, C. A. Donnelly, C. Overstreet, and M. A. Kasevich, Matter Wave Lensing to Picokelvin Temperatures, Phys. Rev. Lett. 114, 143004 (2015).

[41] R. Corgier, S. Loriani, H. Ahlers, K. Posso-Trujillo, C. Schubert, E. M. Rasel, E. Charron, and N. Gaaloul, Inter-acting quantum mixtures for precision atom interferometry, New J. Phys. 22, 123008 (2020).

[42] C. Deppner, W. Herr, M. Cornelius, P. Stromberger, T. Sternke, C. Grzeschik, A. Grote, J. Rudolph, S. Herrmann, M. Krutzik, A. Wenzlawski, R. Corgier, E. Charron, D. Guéry-Odelin, N. Gaaloul, C. Lämmerzahl, A. Peters, P. Windpassinger, and E. M. Rasel, Collective-Mode Enhanced Matter-Wave Optics, Phys. Rev. Lett. 127, 100401 (2021).

[43] D. Leibfried et al., Creation of a six-atom Schrödinger cat state, Nature (London) 438, 639 (2005).

[44] E. Davis, G. Bentsen, and M. Schleier-Smith, Approaching the Heisenberg Limit without Single-Particle Detection, Phys. Rev. Lett. 116, 053601 (2016).

[45] F. Fröwis, P. Sekatski, and W. Dür, Detecting Large Quantum Fisher Information with Finite Measurement Precision, Phys. Rev. Lett. 116, 090801 (2016).

[46] T. Macrì, A. Smerzi, and L. Pezzè, Loschmidt echo for quantum metrology, Phys. Rev. A 94, 010102(R) (2016).

[47] O. Hosten, R. Krishnakumar, N. J. Engelsen, and M. A. Kasevich, Quantum phase magnification, Science 352, 1552 (2016).

[48] S. P. Nolan, S. S. Szigeti, and S. A. Haine, Optimal and Robust Quantum Metrology Using Interaction-Based Read-outs, Phys. Rev. Lett. 119, 193601 (2017).

[49] F. Anders, L. Pezzè, A. Smerzi, and C. Klempt, Phase magnification by two-axis countertwisting for detection-noise robust interferometry, Phys. Rev. A 97, 043813 (2018).

[50] S. A. Haine, Using interaction-based readouts to approach the ultimate limit of detection-noise robustness for quantum-enhanced metrology in collective spin systems, Phys. Rev. A 98, 030303(R) (2018).

[51] M. Schulte, V. J. Martínez-Lahuerta, M. S. Scharnagl, and K. Hammerer, Ramsey interferometry with generalized one-axis twisting echoes, Quantum 4, 268 (2020).

[52] Raman pulses create a superposition between two internal states of an atom: $|g\rangle \equiv |1, 0\rangle$ and $|e\rangle \equiv |2, 2\hbar k_L\rangle$, where the atom in the internal state 2 acquires a momentum kick $2\hbar k_L$, $k_L$ being the wave-vector of the laser. Conversely, Bragg pulses create a superposition between two momentum states, $|g\rangle \equiv |1, 0\rangle$ and $|e\rangle \equiv |1, 2\hbar k_L\rangle$, where the internal state is unchanged.

[53] For sake of simplicity, we introduce the SU(2) pseudo-spin operators of Lie's algebra, $\hat{S}_x = (\hat{a}_g^\dagger \hat{a}_e + \hat{a}_e^\dagger \hat{a}_g)/2$, $\hat{S}_y = (\hat{a}_g^\dagger \hat{a}_e - \hat{a}_e^\dagger \hat{a}_g)/2i$, and $\hat{S}_z = (\hat{a}_g^\dagger \hat{a}_g - \hat{a}_e^\dagger \hat{a}_e)/2$ satisfying the commutation relation $[S_i, S_j] = i\epsilon_{ijk}S_k$ with $\epsilon_{ijk}$ as the Levi-Civita symbol.

[54] See Supplemental Material at http://link.aps.org/supplemental/10.1103/PhysRevLett.127.183401 for details on the derivation of Eq. (1) and Eq. (5) and a discussion about the impact of the DKS on the momentum state of the matter-waves, including possible methods to compensate for this effect, which includes Refs [55–57].

[55] Y. Castin and R. Dum, Bose-Einstein Condensates in Time Dependent Traps, Phys. Rev. Lett. 77, 5315 (1996).

[56] Yu. Kagan, E. L. Surkov, and G. V. Shlyapnikov, Evolution of a Bose gas in anisotropic time-dependent traps, Phys. Rev. A 55, R18(R) (1997).

[57] F. Fitzek, J-N. Siemss, S. Seckmeyer, H. Ahlers, E M. Rasel, K. Hammerer, and N. Gaaloul, Universal atom interferometer simulation of elastic scattering processes, Sci. Rep. 10, 22120 (2020).

[58] This assumption holds in the case of Rubidium-87 species in the hyperfine states $|g\rangle \equiv |F = 1, m_F = -1\rangle$ and $|e\rangle \equiv |F = 2, m_F = 1\rangle$, where $a_{11} = 100.4a_0$, $a_{12} = 97.7a_0$, and $a_{22} = 95.0a_0$ with $a_0$ the Bohr radius.

[59] Q. Guan, T. M. Bersano, S. Mossman, P. Engels, and D. Blume, Rabi oscillations and Ramsey-type pulses in ultracold bosons: Role of interactions, Phys. Rev. A **101,** 063620 (2020).

[60] R. Corgier, L. Pezzè, and A. Smerzi, Nonlinear Bragg trap interferometer, Phys. Rev. A **103,** L061301 (2021).

[61] R. Roy, A. Green, R. Bowler, and S. Gupta, Rapid cooling to quantum degeneracy in dynamically shaped atom traps, Phys. Rev. A **93,** 043403 (2016).

[62] G. Condon, M. Rabault, B. Barrett, L. Chichet, R. Arguel, H. Eneriz-Imaz, D. Naik, A. Bertoldi, B. Battelier, P. Bouyer, and A. Landragin, All-Optical Bose-Einstein Condensates in Microgravity, Phys. Rev. Lett. **123,** 240402 (2019).

[63] This atomic lens is comparable to delta-kick collimation realizations [37–42] with the difference that it targets a focusing of the atomic ensemble and not a collimation. The experimental implementation of one or the other regime follows controlling the duration of the potential flashing.

[64] A. Roura, Circumventing Heisenberg's Uncertainty Principle in Atom Interferometry Tests of the Equivalence Principle, Phys. Rev. Lett. **118,** 160401 (2017).

[65] G. D'Amico, G. Rosi, S. Zhan, L. Cacciapuoti, M. Fattori, and G. M. Tino, Canceling the Gravity Gradient Phase Shift in Atom Interferometry, Phys. Rev. Lett. **119,** 253201 (2017).

[66] C. Overstreet, P. Asenbaum, T. Kovachy, R. Notermans, J. M. Hogan, and M. A. Kasevich, Effective Inertial Frame in an Atom Interferometric Test of the Equivalence Principle, Phys. Rev. Lett. **120,** 183604 (2018).

[67] The calculations are shown in the case of a $^{87}$Rb BEC of $N = 10^6$ atoms initially prepared in a $2\pi\{150, 150, 50\}$ Hz harmonic trap. The BEC is then released from the trap for $T_0 = 5$ ms to insure low interacting ensemble. The DKS pulse is generated by switching on and off the same harmonic trap.

[68] D. J. Wineland, J. J. Bollinger, W. M. Itano, and D. J. Heinzen, Squeezed atomic states and projection noise in spectroscopy, Phys. Rev. A **50,** 67 (1994).

[69] The different phases accumulated during the state preparation, interferometry, and nonlinear readout are assumed to be known and compensate through a careful beam-splitting angle and phase, respectively, at BS2, BS3, and BS4 (as shown, for instance, in Ref. [31]). Here the sensitivity gain of the interferometer is therefore evaluated at $\theta = 0$.

[70] The calculations have been made for $T_0 = 5$ ms, $T_\tau = 5$ ms, $\Delta t_1 = 0.6$ ms, $T'_\tau = 0$, $T_{-\tau} = 1$ ms, and $T'_{-\tau} = 2$ ms for (c) and $T'_{-\tau} = 10$ ms for (d). In both configuration the clouds are diluted enough at each laser pulse to guarantee ideal beam splitters or mirrors pulse efficiencies.

[71] M. Gärttner, J. G. Bohnet, A. Safavi-Naini, M. L. Wall, J. J. Bollinger, and A. M. Rey, Measuring out-of-time-order correlations and multiple quantum spectra in a trapped-ion quantum magnet, Nat. Phys. **13,** 781 (2017).

[72] Y. Li, Y. Castin, and A. Sinatra, Optimum Spin Squeezing in Bose-Einstein Condensates with Particle Losses, Phys. Rev. Lett. **100,** 210401 (2008).

[73] Y. Li, P. Treutlein, J. Reichel, and A. Sinatra, Spin squeezing in a bimodal condensate: Spatial dynamics and particle losses, Eur. Phys. J. B **68,** 365 (2009).

[74] U. V. Poulsen Schulte and K. Mølmer, Quantum beam splitter for atoms, Phys. Rev. A **65,** 033613 (2002).

[75] A. Burchianti, C. D'Errico, L. Marconi, F. Minardi, C. Fort, and M. Modugno, Effect of interactions in the interference pattern of Bose-Einstein condensates, Phys. Rev. A **102,** 043314 (2020).

[76] L. Pezzè, A. Smerzi, G. P. Berman, A. R. Bishop, and L. A. Collins, Nonlinear beam splitter in Bose-Einstein-condensate interferometers, Phys. Rev. A **74,** 033610 (2006).

[77] C. Freier, M. Hauth, V. Schkolnik, B. Leykauf, M. Schilling, H. Wziontek, H.-G. Scherneck, J. Müller, and A. Peters, Mobile quantum gravity sensor with unprecedented stability, J. Phys. Conf. Ser. **723,** 012050 (2016).

[78] R. Karcher, A. Imanaliev, S. Merlet, and F. Pereira Dos Santos, Improving the accuracy of atom interferometers with ultracold sources, New J. Phys. **20,** 113041 (2018).

[79] B. Battelier *et al.*, Exploring the foundations of the Universe with space tests of the equivalence principle, arXiv:1908.11785.

[80] G. M. Tino, L. Cacciapuoti, S. Capozziello, G. Lambiase, and F. Sorrentino, Precision gravity tests and the Einstein equivalence principle, Prog. Part. Nucl. Phys. **112,** 103772 (2020).

[81] B. Canuel *et al.*, ELGAR—a European laboratory for gravitation and atom-interferometric research, Classical Quantum Gravity **37,** 225017 (2020).